Fermi National Accelerator Laboratory

FERMILAB-Pub-98/232-A

An Accurate Calculation of the Big-Bang Prediction for the Abundance of Primordial Helium

Robert E. Lopez and Michael S. Turner

Fermi National Accelerator Laboratory
P.O. Box 500, Batavia, Illinois 60510

August 1998

Submitted to *Physical Review D*

Operated by Universities Research Association Inc. under Contract No. DE-AC02-76CH03000 with the United States Department of Energy

Disclaimer

Distribution

Fermilab–Pub–98/232A
astro-ph/9807279
submitted to *Physical Review D*

An Accurate Calculation of the Big-Bang Prediction for the Abundance of Primordial Helium

Robert E. Lopez[1,2] and Michael S. Turner[1,2,3]

[1]*Department of Physics,*
The University of Chicago, Chicago, IL 60637-1433
[2]*NASA/Fermilab Astrophysics Center,*
Fermi National Accelerator Laboratory, Batavia, IL 60510-0500
[3]*Department of Astronomy & Astrophysics,*
Enrico Fermi Institute, The University of Chicago, Chicago, IL 60637-1433

ABSTRACT

Within the standard model of particle physics and cosmology we have calculated the big-bang prediction for the primordial abundance of Helium to a theoretical uncertainty of 0.1% ($\delta Y_P = \pm 0.0002$). At this accuracy the uncertainty in the abundance is dominated by the experimental uncertainty in the neutron mean lifetime, $\tau_n = 885.3 \pm 2.0\,\mathrm{sec}$. The following physical effects were included in the calculation: the zero and finite-temperature radiative, Coulomb and finite-nucleon mass corrections to the weak rates; order-α quantum-electrodynamic correction to the plasma density, electron mass, and neutrino temperature; and incomplete neutrino decoupling. New results for the finite-temperature radiative correction and the QED plasma correction were used. In addition, we wrote a new and independent nucleosynthesis code to control numerical errors to less than 0.1%. Our predictions for the ^{4}He abundance are summarized with an accurate fitting formula. Summarizing our work in one number, $Y_P(\eta = 5 \times 10^{-10}) = 0.2460 \pm 0.0004$ (expt) $\pm <$ 0.0002 (theory).

1 Introduction

Big-bang nucleosynthesis (BBN) is one of the observational pillars of the standard cosmology, and has the potential to be a precision probe of the early universe and fundamental physics [1, 2, 3]. Observations of light-element abundances have improved dramatically over the past few years, and the current and planned precision measurements of Deuterium, Helium-4, Helium-3 and Lithium-7, should allow a precise (10% or better) determination of the baryon density and consistency check of BBN, but only if the theoretical predictions of the light element abundances are as good as the observations. In particular, a measurement of the primeval Deuterium abundance pins down the baryon density, and in turn the other three abundances. Because the subsequent evolution of the ^{4}He abundance is simple - stars make Helium - and measurements have the potential of determining Y_P to three significant figures, Helium can provide an important consistency check of BBN. Furthermore, an independent determination of the baryon density from cosmic microwave background anisotropies will soon test the consistency of the standard model of cosmology. Finally, the combination of accurate observations and theory can be used to test physics beyond the standard model of particle physics [1, 4], e.g., by imposing a strict limit on the number of light neutrino species [5, 6, 7]. Cosmology is entering a high precision age, and this motivates high-precision BBN.

Over the years, theoretical study of Helium formation has been intense, with the following effects being considered: Coulomb and radiative corrections to the weak rates [8, 9, 10, 11, 12, 13], BBN code numerical errors [11], nuclear reaction rate uncertainties [14, 15], finite-temperature QED plasma corrections [8, 16], the effect of finite-nucleon mass [17, 18], and incomplete neutrino decoupling [8, 19].

The goal of this work was a calculation of the primordial abundance of Helium, within the standard models of particle physics and cosmology, accurate enough so that its uncertainty is dominated by the experimental uncertainty in the neutron mean lifetime[1], $\tau_n = 885.3 \pm 2.0$ sec [20, 21, 22]. Because τ_n is so accurately known ($\delta\tau_n/\tau_n = 0.23\%$), it is used to normalize all of the weak rates that interconvert neutrons and protons: $\epsilon p \leftrightarrow \nu n$, $\epsilon^+ n \leftrightarrow \bar{\nu} p$ and $n \leftrightarrow p\epsilon\bar{\nu}$. The baryon-number fraction of ^{4}He produced ($\equiv Y_P$) depends sensitively on the weak rates because they determine the neutron-to-proton ratio n/p before nucleosynthesis, and essentially all of the neutrons around at the onset of nucleosynthesis go into forming ^{4}He. We have determined the effect on Y_P by perturbing the weak rates in the standard code [23],

$$\frac{\delta Y_P}{Y_P} \simeq -0.8 \frac{\delta\Gamma}{\Gamma}. \tag{1}$$

Since the weak rates scale as $1/\tau_n$, this estimate implies that $\delta\tau_n$ introduces an uncertainty in Y_P of 0.18%. We use this uncertainty to set our goal for all theoretical uncertainty.

To meet our goal we need to calculate the weak rates to precision of better than 0.23 %. Another source of errors in Y_P come from thermodynamics, i.e., the energy density ρ, the pressure P and the

[1]The Particle Data Group currently recommends $\tau_n = 887 \pm 2$ sec [20]. A recent measurement using ultracold neutrons obtains a slightly lower value, $\tau_n = 885.3 \pm 0.9\text{stat} \pm 0.4\text{sys}$ [21]. For our central value we use 885.3 and for the uncertainty we use ± 2 sec.

neutrino temperature T_ν. To determine how accurately we need to know thermodynamic quantities, we can estimate the change in Y_P due to a change in a thermodynamic quantity, e.g., ρ. Again, using the standard code, we find

$$\frac{\delta Y_P}{Y_P} \simeq 0.4 \frac{\delta\rho}{\rho}, \tag{2}$$

This indicates that we should calculate thermodynamic quantities to better than 0.45%.

When calculating Y_P to this precision, several factors must be considered:

1. Weak rate and thermodynamics numerics: most quantities to be calculated involve integrations that must be done numerically.

2. ODE integration numerics: nucleosynthesis codes contain finite stepsize errors.

3. Nuclear reaction rates: errors originate from experimental uncertainties in the nuclear reaction data, as well as from neglecting nuclear reactions important to BBN.

4. Weak-rate physics: there are several small physical effects that must be calculated, including Coulomb, zero and finite-temperature radiative corrections, and the effect of finite-nucleon mass.

5. Thermodynamics physics: for temperatures much greater than the electron mass, there are order-α quantum electrodynamic corrections to the equation of state of the plasma.

6. Incomplete neutrino decoupling: neutrinos share partially in the entropy release when $\epsilon^\pm$ pairs annihilate.

Items 1, 2 and 3 are addressed in the next section; item 4 is addressed in Sec. 3. Items 5 and 6 are taken up in Sec. 4, and a summary of our results is given in the final section.

Finally, we mention that we have not considered the $\mathcal{O}(\alpha^{3/2})$ collective plasma effects due to the presence of the copious numbers of $\epsilon^\pm$ pairs at the time of BBN, because they are safely below our theoretical error budget of 0.l% for Y_P. These effects, all of relative size 0.1% and calculated in Ref. [24], are: the enhancement of nuclear reaction rates due to Debye screening of nuclear charge; the contribution of longitudinal plasmon modes ($k \lesssim \omega_p \sim 4\pi n_{\epsilon^\pm}/T$) to the energy density and pressure; the (negative) contribution to the energy density and pressure of the electromagnetic interaction of $\epsilon^\pm$ pairs; and the reduction of the energy and pressure of photons due to plasma effects on low frequency photons ($k \lesssim \omega_p$).

2 Numerics

2.1 BBN Code

We have written a new nucleosynthesis code that is independent of the standard (Kawano) code [23]. The heart of any nucleosynthesis code is the set of ordinary differential equations that govern the evolution of the abundances of the light elements (see, e.g., Ref. [25, 26]). This code tracks protons,

neutrons, Deuterium (D), Tritium (T), Helium-3 (^{3}He), Helium-4 (^{4}He), Lithium-6 (^{6}Li), Lithium-7 (^{7}Li) and Beryllium-7 (^{7}Be). The baryon-number fraction of element i is given by[2]

$$X_i = \frac{A_i n_i}{n_B}, \tag{3}$$

where A_i is the element's atomic number, n_i it's number density, and n_B is the baryon-number density. Nuclear reaction rates govern the evolution of the elemental abundances. Conservation of baryon number provides the constraint:

$$\sum_i X_i = 1. \tag{4}$$

We take for our initial temperature, $T_i = 10$ MeV, and for our initial abundances, the nuclear statistical equilibrium (NSE) values:

$$X_A = g_A \left[\zeta(3)^{A-1}\pi^{(1-A)/2}2^{(3A-5)/2}\right] A^{5/2} \left(\frac{T}{m_N}\right)^{3(A-1)/2} \eta^{A-1} X_p^Z X_n^{A-Z} \epsilon^{B_A/T} \tag{5}$$

where A is the atomic number, $m_N \simeq 940\,\mathrm{MeV}$ is the nuclear mass, η is the baryon-to-photon ratio, B_A is the binding energy of species A, and $\zeta(3) \simeq 1.20206$. At temperatures greater than about an MeV, the nuclear rates are sufficiently high to cause the abundances to rapidly assume their NSE values. If we make the reasonable assumption that the elements are always in kinetic equilibrium, then the rate coefficients depend only on η and T. This implies the important and well known conclusion that the predictions of nucleosynthesis are a function of only one parameter, η, which is equivalent to n_B since $T_\gamma = 2.7277 \pm 0.002$ K is so well known.

Several important quantities enter into the evolution equations: weak rates, thermodynamic quantities and nuclear reaction rates. For the weak rates, we define the total conversion rates (per neutron or proton):

$$\begin{aligned} \Gamma_{n\to p} &\equiv \Gamma_{e^+\, n\to\bar{\nu}\, p} + \Gamma_{\nu\, n\to e\, p} + \Gamma_{n\to p\, e\, \bar{\nu}}\,, \\ \Gamma_{p\to n} &\equiv \Gamma_{e\, p\to\nu\, n} + \Gamma_{\bar{\nu}\, p\to e^+\, n} + \Gamma_{p\, e\, \bar{\nu}\to n}\,. \end{aligned} \tag{6}$$

Simple expressions for these rates may be obtained assuming no radiative corrections and infinite nucleon mass. The thermodynamic quantities that must be calculated are $\rho(T)$, $T_\nu(T)$, $\rho_B(T)$ and the differential time-temperature relation dt/dT.

[2]Baryon-number fraction and baryon-mass fraction differ by order 1% due to nuclear binding energy. Because nuclear reactions change the total mass in baryons, the mass fraction of species A_i ($\equiv X_i^{mass}$) can change even if the number of species A_i does not. The mass fraction of species A_i is

$$X_i^{mass} = \frac{n_i m_i}{\sum_j n_j m_j} = \frac{n_i}{n_H}\,\frac{m_i}{m_H}\,\frac{1}{1+\sum_j (n_j/n_H)\,(m_j/m_H)}\,,$$

where m_i is the mass of species i: (e.g., $m_4 = 4.002602\,$amu) and $m_H = 1.00783\,$amu. In the expression for X_i, m_i/m_H is replaced by A_i. For $Y_P = 0.25$ and the primordial mix of elements $X_4^{mass} = 0.24866$. Similarly, the relationship between the baryon mass density and η depends on elemental composition. For the primordial mix with $Y_P = 0.25$,

$$\Omega_B h^2 = 3.66 \times 10^7\, \eta,$$

assuming $T_\gamma = 2.7277\,K$. Assuming a mass of 1 amu per nucleon, the prefactor is 3.639×10^7, and for the solar abundance the prefactor is 3.66043×10^7.

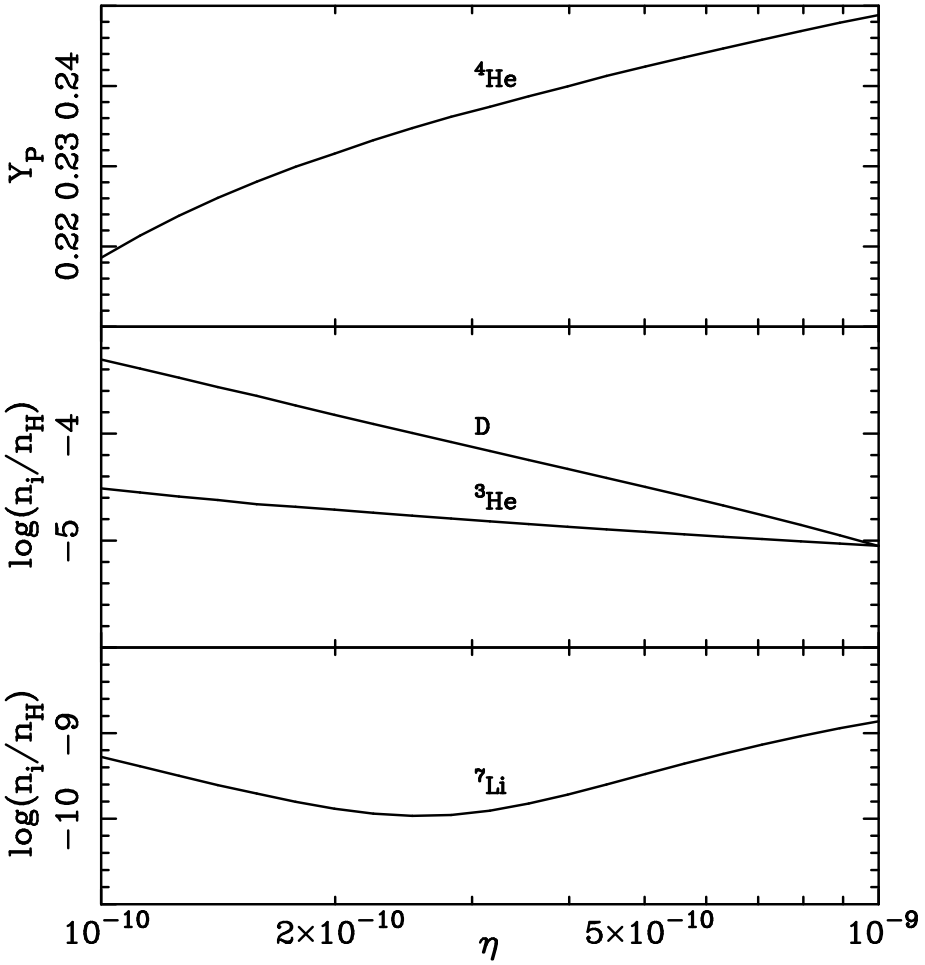

Figure 1: Baseline of "final" predictions: element abundances predicted by our BBN code.

1)	p + n	$\leftrightarrow$	D + γ
2)	D + n	$\leftrightarrow$	T + γ
3)	^{3}He + n	$\leftrightarrow$	^{4}He + γ
4)	^{6}Li + n	$\leftrightarrow$	^{7}Li + γ
5)	^{3}He + n	$\leftrightarrow$	T + p
6)	^{7}Be + n	$\leftrightarrow$	^{7}Li + p
7)	^{7}Li + n	$\leftrightarrow$	^{3}He + ^{4}He
8)	^{7}Be + n	$\leftrightarrow$	^{4}He + ^{4}He
9)	D + p	$\leftrightarrow$	^{3}He + γ
10)	T + p	$\leftrightarrow$	^{4}He + γ
11)	^{6}Li + p	$\leftrightarrow$	^{7}Be + γ
12)	^{7}Li + p	$\leftrightarrow$	^{4}He + ^{4}He
13)	D + ^{4}He	$\leftrightarrow$	^{6}Li + γ
14)	T + ^{4}He	$\leftrightarrow$	^{7}Li + γ
15)	^{3}He + ^{4}He	$\leftrightarrow$	^{7}Be + γ
16)	D + D	$\leftrightarrow$	^{3}He + n
17)	D + D	$\leftrightarrow$	T + p
18)	D + T	$\leftrightarrow$	^{4}He + p
19)	D + ^{3}He	$\leftrightarrow$	^{4}He + n
20)	^{3}He + ^{3}He	$\leftrightarrow$	^{4}He + p + p
21)	D + ^{7}Li	$\leftrightarrow$	^{4}He + ^{4}He + n
22)	D + ^{7}Be	$\leftrightarrow$	^{4}He + ^{4}He + p

Table 1: Reactions used in our code.

Our BBN code is completely independent from the standard code, with one exception. Our code uses the same nuclear-rate data (with the exception of the weak rates). The nuclear-reaction network corresponds to the smallest one offered by the standard code, which contains the reactions listed in Table 1. Although this network is much smaller than the largest offered in the standard code, the effect on Y_P from neglecting these additional reactions is less than 10^{-4}. The light-element abundances predicted by our code are shown in Fig. 1.

2.2 Numerical Accuracy of the BBN Codes

Because the differential equations governing the light-element abundances are stiff, an implicit integrator was used to evolve them. Instead of entering explicit time steps, as in the standard code, the desired final accuracies are entered as parameters of our code's integrator. The temperature steps are then determined adaptively. Integrator accuracy parameters are chosen to be small enough so that stepsize errors were much smaller than the allowed error in Y_P.

To calculate the weak rates and thermodynamic quantities accurately, we proceed as follows (see, e.g., Ref. [27]). Let $I = \int_a^b f(x)\,dx$ for some function $f(x)$. Expressed as a first order ordinary differential equation, $I = J(b)$ where $dJ/dx = f(x)$, $J(a) = 0$. We solve this differential equation using a fourth order Runge-Kutta routine. Figure 2 demonstrates for a specific example that the actual numerical errors are as small as requested. All of the weak rates and thermodynamic

	Y_P
1. standard code with default stepsize	0.2348
2. standard code with small stepsize	0.2415
3. our code	0.2411

Table 2: Comparison of the standard code and our code for $\eta = 5.0 \times 10^{-10}$. The two stepsize parameters in the standard code are 0.3 and 0.6, respectively. The difference between 1. and 2., $\delta Y_P = 0.0073$, is the integration error for these stepsizes; the small difference between 2. and 3., $\delta Y_P = 0.0004$, shows that our code agrees with the standard code to within 0.2%. When very accurate weak-rate routines are inserted into the standard code the agreement improves to about 0.1%.

quantities were calculated so that their numerical error contributions to the uncertainty in Y_P were acceptably small.

We compared the output of our code to the standard code, which dates back to the original version written in 1966 [25], updated by Wagoner in 1973 [26, 28], and modernized and made user friendly in 1988 [29]. Nuclear reaction rates were updated in 1993[14]. One must be careful when making comparisons. First one must consider the numerical accuracy of the standard code. Kernan and Krauss reported finding a significant numerical error in the standard code [11, 30], $\delta Y_P = 0.0017$, large enough to be very significant at our level of accuracy. Second, the standard code implements certain physics corrections, namely a Coulomb correction put in by Wagoner. He approximates the Coulomb correction by scaling all of the weak rates a factor, 0.98, independent of temperature.

The Kernan-Krauss correction was measured by comparing the predictions of the standard code at some unspecified integration stepsize to the predictions as the stepsize became very small; note, however, that the error using the default stepsize (in Ref. [23]) is four times larger. It is added to the results at the end of the computation. Needless to say, a simple additive numerical correction is not adequate because other codes exist and not all users of the standard code use the same stepsize. For our comparison we took out the Kernan and Coulomb corrections and then made the stepsizes small enough so that integration errors were negligable. With the standard code configured this way, we compared Y_P and D as a function of η in two scenarios. For the first, we used the standard weak rate routines to calculate the weak rates. For the second we used our high precision weak rate routines to calculate the weak rates in the standard code. The results are shown in Table 2 and Fig. 3. The agreement is excellent: for Y_P the codes differ by less than 0.15% with our weak-rate routines and by less than 0.2% with the standard weak rate routines. For D the codes agree to better than 0.75%.

This agreement gave us confidence that our code calculates Y_P accurately for the baseline case (without the physics corrections). Of course, the convergence of two independent codes is not proof that they converge on the correct value. Since our code was the first that was designed and engineered around an error budget, we will take it and its internal error budget as the baseline for all further calculations.

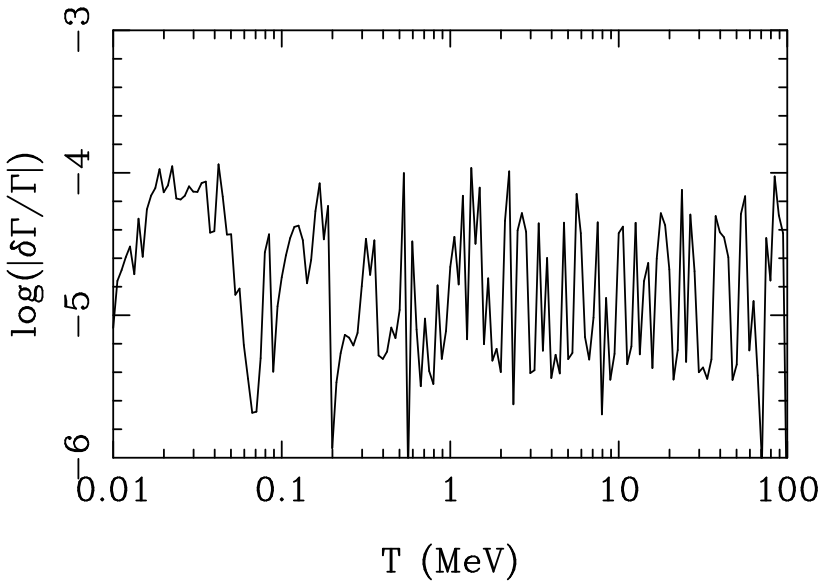

Figure 2: Numerical error calculating $\Gamma_{ep\to\nu n}$ for error parameter set at $\delta\Gamma/\Gamma = 10^{-4}$. The error is acceptable low for all temperatures. Similar results were obtained for the other weak rates and thermodynamic quantities.

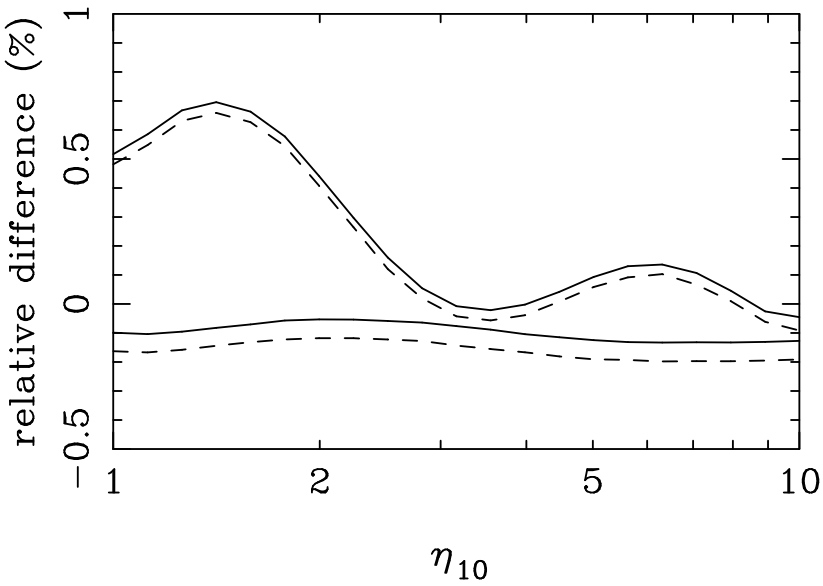

Figure 3: Comparison between the standard code and our code for Helium-4 (lower curves) and deuterium (upper curves). For the solid curves, our very accurate weak rates were inserted into the standard code. For the dashed curves, the stamdard code's weak rate routines were used in the standard code. ($\eta_{10} \equiv \eta/10^{-10}$)

Reaction k	$\delta R_k/R_k$	$\delta Y_P/Y_P$ ($\eta_{10}=5.0$)	$\delta Y_P/Y_P$ ($\eta_{10}=1.8$)
$n \leftrightarrow p$	0.23%	0.17%	0.18%
$p(n,\gamma)d$	7%	0.04%	0.17%
$d(d,n)^3He$	10%	0.06%	0.07%
$d(d,p)T$	10%	0.05%	0.06%
Total Uncertainty		0.19%	0.27%

Table 3: 1-σ experimental uncertainties and their effect on Y_P. All nuclear rates whose uncertainties significantly impact Y_P are shown. The weak-rate uncertainty of 0.23% is due to uncertainty in measurements of the neutron mean lifetime, and assumes that Coulomb, radiative and thermodynamic corrections to the weak rates are known to better accuracy than this. Note that for $\eta = 5.0 \times 10^{-10}$, the weak rates dominate the error budget. The bottom row indicates the RMS total uncertainty in Y_P for these two values of η.

2.3 Nuclear Rate Uncertainties

The primordial Helium abundance is sensitive to nuclear reactions other than the weak rates. Several studies of the uncertainties in theoretical abundances due to nuclear rate uncertainties have been performed [1, 14, 30, 31, 32, 33]. Here we will use the results and techniques of the recent work of Fiorentini, et al [15]. They use linear error propagation theory to quantify the effect of experimental uncertainties in the nuclear-reaction rates on the light element abundance uncertainties and their correlations. In this formalism the uncertainty in the Helium abundance is given by

$$\left(\frac{\delta Y_P}{Y_P}\right)^2 = \sum_k \lambda_k^2 \, \delta R_k^2 \, , \tag{7}$$

where the sum k is over nuclear rates, δR_k is the experimental relative uncertainty in the rate R_k, and λ_k is the logarithmic derivative

$$\lambda_k = \frac{\partial \log Y_P}{\partial \log R_k}. \tag{8}$$

Fiorentini, et al [15] calculate the logarithmic derivatives numerically, using the standard code. The experimental rate uncertainties are taken from Smith, et al [14]. Contributions to the uncertainty in the Helium abundance arise almost entirely from four rates. Table 2.3 lists these rates and their relative experimental uncertainties. Figure 4 shows the resulting uncertainty in Y_P. At low values of η is appears that the reaction $p(n,\gamma)d$ dominates the error budget. However, it should be noted that the quoted experimental uncertainties for the reactions other than $n \leftrightarrow p$ are very conservative, perhaps overestimating the true uncertainties by a factor of several [34]. Furthermore, for $\eta = 5 \times 10^{-10}$, which is implied by by measurements of the primeval D abundance[35], the weak rates dominate the error budget even for these conservative uncertainties. In any case, it is important to reduce the theoretical error budget wherever possible, and to accurately quantify its size.

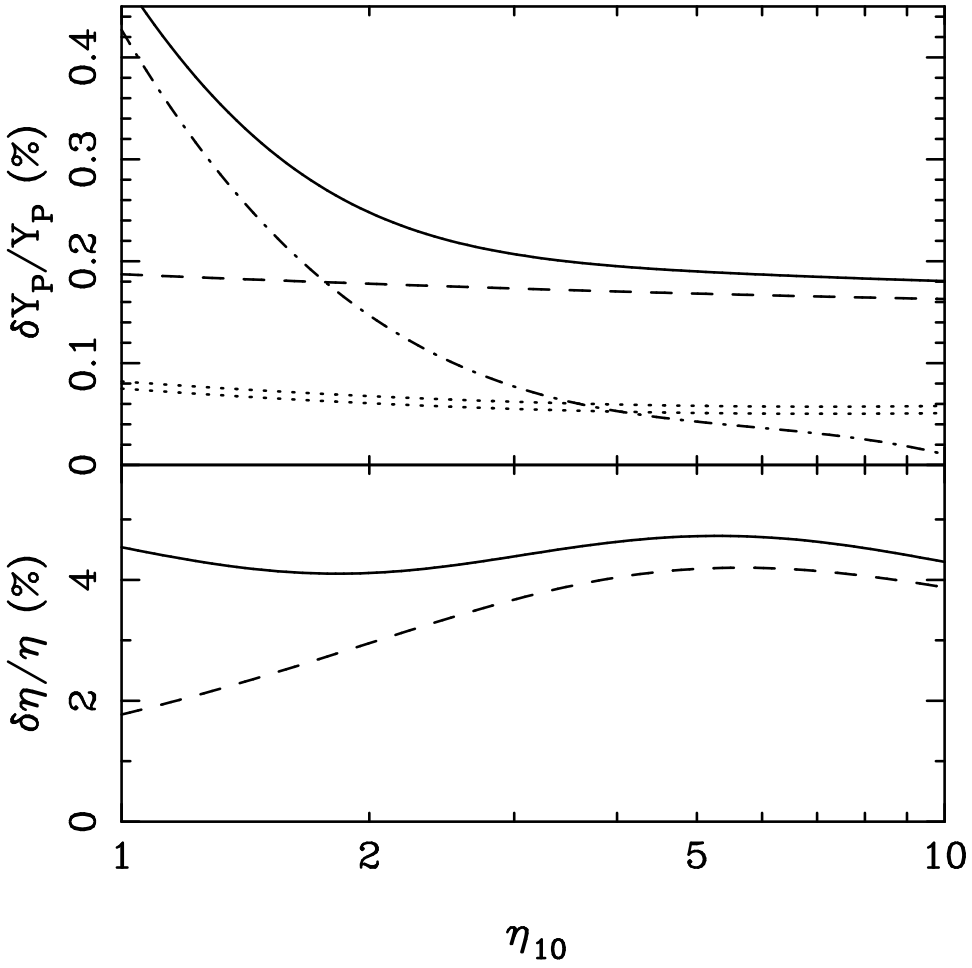

Figure 4: The top panel shows the uncertainty in Y_P due to experimental uncertainties in nuclear rates, as a function of η. The solid line shows the total uncertainty, while the other lines show each nuclear reaction separatley. The dashed line is for $n \leftrightarrow p$, the dashed-dotted line is for $p(n,\gamma)d$, and the two dotted lines are for $d(d,n)^3$He and $d(d,p)$T. The bottom panel shows the uncertainty in η that would result from the above uncertainties in Y_P, when η is derived from the ^{4}He abundance. The dashed line is for the weak rate uncertainties alone, while the solid line is for the total nuclear rate uncertainty. The factor of ten difference in the scales between the two panels is indicative of the fact that Y_P depends logarithmically upon η.

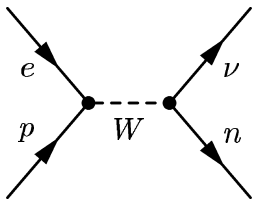

Figure 5: Tree level diagram for the process $ep \to \nu n$.

3 Weak Rates

The primordial helium abundance is very sensitive to the weak rates that interconvert neutrons and protons. To calculate Y_P to 0.12% the weak rates must be known at the 0.15% level. In addition to numerical issues discussed earlier, several physical effects are important at this level: zero-temperature radiative and Coulomb corrections, finite-nucleon mass correction, and finite-temperature radiative correction.

The expressions for the weak rates are derived starting with the tree-level (Born diagram) shown in Fig. 5. For purposes of illustration, we will consider the process $e^- + p \to \nu_e + n$. Without making any approximations the phase space integral for the conversion rate (per proton) can be simplified to a five-dimensional integral involving the matrix-element squared $|\mathcal{M}|^2$ [18]

$$\begin{aligned}
\Gamma_{ep\leftrightarrow\nu n} &= \frac{1}{2^9\pi^6 n_p}\int dp_e dp_p d\cos\theta_p d\cos\theta_\nu d\phi_\nu \\
&\quad \times \frac{p_e^2 p_p^2 E_\nu}{E_e E_p E_n}\frac{1}{\mathcal{J}}\,|\mathcal{M}|^2\, f_e f_p (1-f_\nu)(1-f_n), \qquad (9)\\
\mathcal{J} &= 1+\frac{E_\nu}{E_n}\left(1-\frac{(\mathbf{p}_e+\mathbf{p}_p)\cdot\mathbf{p}_\nu}{E_\nu^2}\right), \qquad (10)
\end{aligned}$$

where E_e, E_p, E_ν, and E_n denote the energies of the respective particles and $\mathcal{J}$ is the Jacobian introduced in integrating the energy part of the delta function. $|\mathcal{M}|^2$ is summed over initial and final state spins. The integration limits correspond to the kinematically allowed region in the five-variable phase space. An expression for E_ν in terms of the integration variables $p_e, p_p, \theta_p, \theta_\nu$, and ϕ_ν is given by

$$\begin{aligned}
p_\nu &= \frac{A^2 B + 2E\sqrt{A^4 - m_\nu^2(4E^2-B^2)}}{4E^2-B^2},\\
A^2 &\equiv 2E_e E_p + m_\nu^2 - m_n^2 - m_e^2 - m_p^2 - 2p_e p_p\cos\theta_p,\\
B &\equiv 2\left[p_e\cos\theta_\nu + p_p\left(\cos\theta_p\cos\theta_\nu + \sin\theta_p\sin\theta_\nu\cos\phi_\nu\right)\right]. \qquad (11)
\end{aligned}$$

where $E = E_e + E_p$. For more details, see Ref. [18].

This rate expression is challenging to evaluate for two reasons. First, the kinematically allowed region in the five-dimensional phase space is not simple. Second, the matrix element is complex. If the nucleons are assumed to be infinitely massive, the expression simplifies greatly. The matrix element $|\mathcal{M}|^2 = 2^5 G_F^2(1+3g_A^2)E_e E_p E_\nu E_n$. The sole kinematical constraint is $E_p = E_\nu + Q$, ($Q =$

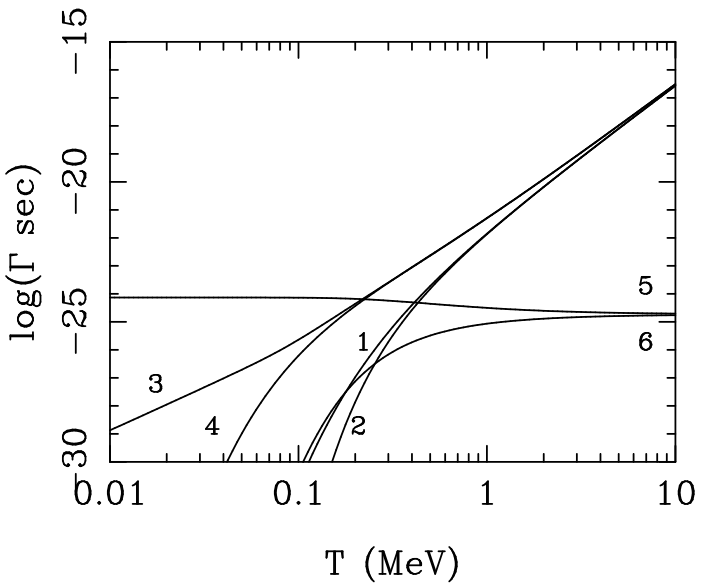

Figure 6: Weak rates as a function of temperature (Born diagram, infinite-nucleon-mass limit): (1) $ep \to \nu n$, (2) $\nu p \to en$, (3) $en \to \nu p$, (4) $\nu n \to ep$, (5) $n \to pe\nu$, (6) $pe\nu \to n$. Note, freeze-out of the n/p ratio occurs at $T \simeq 0.8\,\mathrm{MeV}$ and nucleosynthesis begins in earnest at $T \simeq 0.1\,\mathrm{MeV}$.

$m_n - m_p = 1.293$, MeV), and the rate expression becomes a one variable integration. Normalizing the rates to the zero-temperature free neutron decay rate $1/\tau_n = \Gamma_{n\to pe\nu}(T=0)$,

$$\frac{1}{\tau_n} = \frac{G_F^2(1+3g_A^2)m_e^5}{2\pi^3}\lambda_0, \tag{12}$$

$$\lambda_0 = \int_1^q d\epsilon\, \epsilon(\epsilon-q)^2(\epsilon^2-1)^{1/2} = 1.6333\,, \tag{13}$$

leads to the well known formula for the process $ep \to \nu n$:

$$\Gamma^{\infty}_{ep\to\nu n} = \frac{1}{\tau_n\lambda_0}\int_q^{\infty} \frac{\epsilon(\epsilon^2-q^2)^{1/2}}{[1+\exp(\epsilon z)][1+\exp((q-\epsilon)z_\nu))]}; \tag{14}$$

where T is the photon temperature, T_ν is the neutrino temperature, $\epsilon \equiv E_e/m_e$, $q \equiv Q/m_e$, $z \equiv m_e/T$, and $z_\nu \equiv m_e/T_\nu$. Summing the $n \to p$ and $p \to n$ rates yields the standard weak-rate expressions [36]

$$\Gamma_{n\to p} = \frac{1}{\tau_n\lambda_0}\left(-\int_{-\infty}^{-1} + \int_1^{\infty}\right) d\epsilon \frac{\epsilon(\epsilon-q)^2\sqrt{\epsilon^2-1}}{(1+e^{-\epsilon z})\,(1+e^{(q-\epsilon)z_\nu})},$$

$$\Gamma_{p\to n} = \frac{1}{\tau_n\lambda_0}\left(-\int_{-\infty}^{-1} + \int_1^{\infty}\right) d\epsilon \frac{\epsilon(\epsilon-q)^2\sqrt{\epsilon^2-1}}{(1+e^{\epsilon z})\,(1+e^{(\epsilon-q)z_\nu})}. \tag{15}$$

The six individual rates are plotted as a function of temperature in Fig. 6.

3.1 Zero-Temperature Coulomb and Radiative Corrections

To order α, the weak rates with zero-temperature Coulomb and radiative corrections are given by the sum of the interference between the Born diagram (Fig. 5) and the diagrams in Fig. 7.

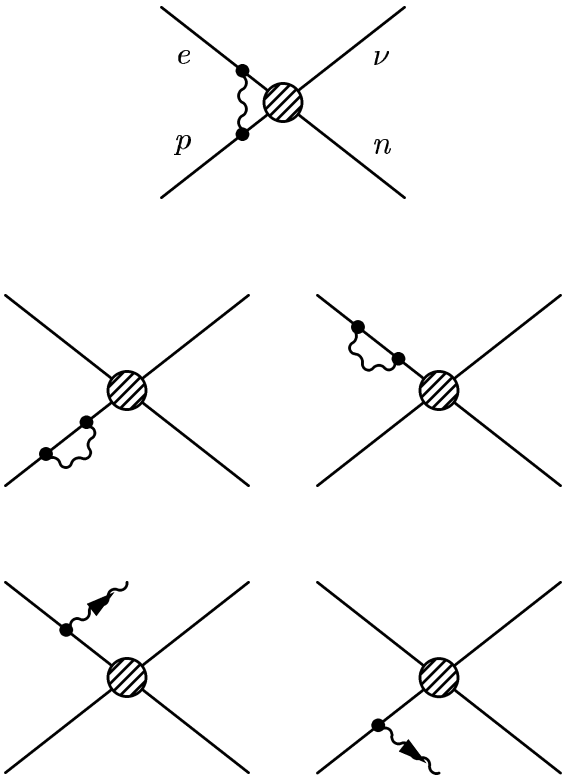

Figure 7: Zero-temperature corrections to the process $\epsilon p \to \nu n$. The center blob is the charged-current, weak-interaction vertex.

It is conventional to separate the corrections into a Coulomb part proportional to nuclear charge $Z\epsilon$ and a radiative part proportional to ϵ. Since $Z = 1$ here, this separation is arbitrary. Dicus et al calculated the Coulomb and zero-temperature radiative corrections to the weak rates in 1982 [8]. Summarizing their results we obtain the following prescription for correcting the rates. First, perform the zero-temperature radiative corrections by multiplying the integrands of all of the rates by the factor,

$$\left[1 + \frac{\alpha}{2\pi} C(\beta, \mathrm{y})\right] , \tag{16}$$

where

$$\begin{aligned} C(\beta, \mathrm{y}) &= 40 + 4(R-1)\left(\frac{y}{3\epsilon} - \frac{3}{2} + \ln 2y\right) + R\left(2(1+\beta^2) + \frac{y^2}{6\epsilon^2} - 4\beta R\right) \\ &\quad -4\left(2 + 11\beta + 25\beta^2 + 25\beta^3 + 30\beta^4 + 20\beta^5 + 8\beta^6\right)/(1+\beta)^6, \end{aligned} \tag{17}$$

β is the electron's velocity and $R = \tanh \beta^{-1}/\beta$. Next apply the Coulomb correction by multiplying the integrand of the rates for $n \leftrightarrow p e \nu$ and $e p \leftrightarrow \nu n$ by the Fermi factor,

$$F(\beta) = \frac{2\pi\alpha/\beta}{1 - \epsilon^{-2\pi\alpha/\beta}}. \tag{18}$$

Here we used the non-relativistic Fermi function. The error from using the non-relativistic version is of order 2% of the Coulomb effect itself [37], and so the approximation is fine. Finally, λ_0 must be corrected for Coulomb and zero-temperature radiative effects by multiplying it's integrand by $\left[1 + \frac{\alpha}{2\pi} C(\beta, \mathrm{y})\right] F(\beta)$. Doing this increases λ_0 by 7.15%, to 1.7501.

Figure 8 shows the combined zero-temperature corrections. Note that the corrections are less than or equal to zero for both rates for all temperatures: decreased weak rates imply earlier n/p freeze-out and an increase in Y_P. Our code calculates the zero-temperature corrections to the weak rates by modifying the integrands of the rate expressions as described above, and by using the corrected λ_0. The zero-temperature corrections yield a change, $\delta Y_P/Y_P = 1.28\%$ which is insensitive to the value of η over the range $10^{-10} \leq \eta \leq 10^{-9}$. This result is in agreement with Ref. [8].

Wagoner approximated the Coulomb correction by reducing both the $n \to n$ and $p \to n$ rates by 2%. This correction, shown by the horizontal line, is close to the high temperature asymptotic Coulomb correction of -2.16%. However, n/p continues to decrease slowly for temperatures lower than freeze-out, where Wagoner's approximation breaks down. The fact that the real corrections are less negative in this regime means that the change in Y_P from the Coulomb correction will be less positive than one would estimate from Wagoner's approximation. Adding in the zero-temperature radiative corrections brings the total zero-temperature change in Y_P closer to what would be found using Wagoner's approximation to the Coulomb correction. Table 3.1 shows $\delta Y_P/Y_P$ for the Coulomb and zero-temperature radiatively separately and summed, compared to $\delta Y_P/Y_P$ from Wagoner's approximation. Note in particular that the difference between Wagoner's approximation and the zero-temperature correction is 0.28%, which is significant at the 0.1% level.

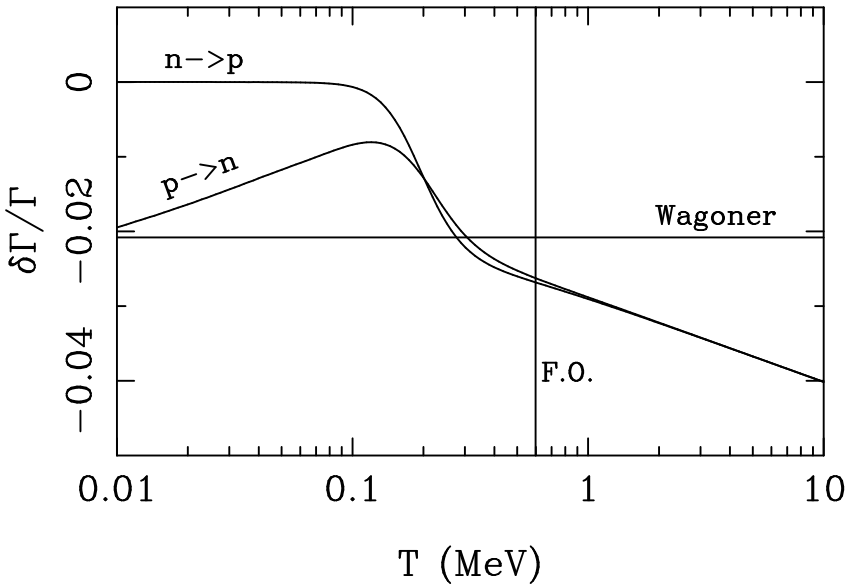

Figure 8: Zero-temperature radiative and Coulomb corrections to the $n \leftrightarrow p$ rates. The horizontal line is Wagoner's approximation to the Coulomb correction. The vertical line is at freeze-out.

Correction	$\delta Y_P/Y_P$
Coulomb	1.04%
T=0 Radiative	0.24%
Combined	1.28%
Wagoner's approximation	1.56%

Table 4: Zero-temperature corrections to Y_P, compared with change in Y_P from Wagoner's approximation of the Coulomb correction. These corrections are insensitive to η for $10^{-10} \leq \eta \leq 10^{-9}$.

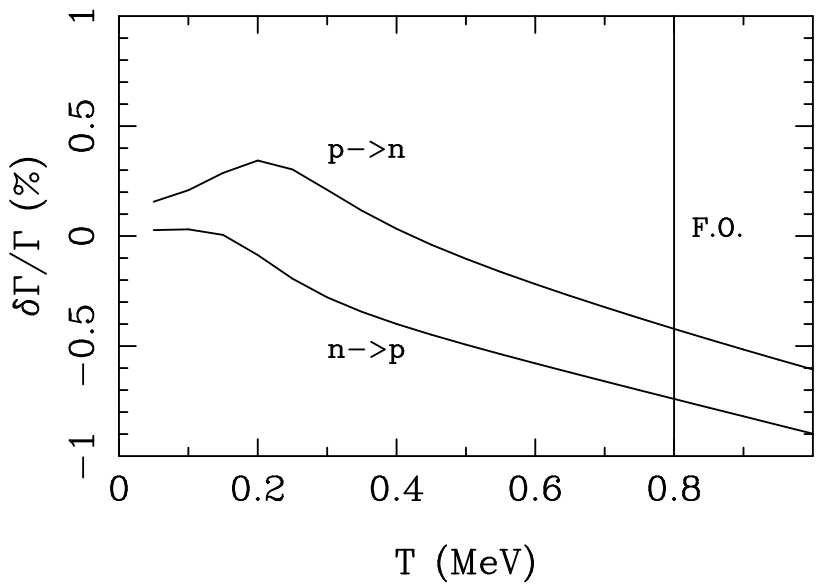

Figure 9: Finite-nucleon-mass correction to the $n \leftrightarrow p$ rates. The freeze-out temperature, $T_F \simeq 0.8\,\mathrm{MeV}$, is indicated with a vertical line.

3.2 Finite-Nucleon Mass Correction

Recall that the standard rate expressions, Eqn. 14, assume infinitely massive nucleons. We have calculated the weak rates without this assumption by numerically integrating the five-dimensional rate integral, Eq. 9, using the Monte Carlo method [18]. Figure 9 shows the finite-mass corrections to the $n \leftrightarrow p$ rates. Using the individual rate corrections we found the corrections to the summed $n \leftrightarrow p$ rates,

$$\frac{\delta\Gamma_{n\to p}}{\Gamma_{n\to p}} \equiv \frac{\Gamma_{n\to p} - \Gamma^{\infty}_{n\to p}}{\Gamma^{\infty}_{n\to p}} \tag{19}$$

$$\frac{\delta\Gamma_{p\to n}}{\Gamma_{p\to n}} \equiv \frac{\Gamma_{p\to n} - \Gamma^{\infty}_{p\to n}}{\Gamma^{\infty}_{p\to n}}, \tag{20}$$

where Γ^{∞} is the rate in the infinite-mass approximation, and Γ is the unapproximated rate. Our corrections are accurate to within a few percent, and were verified several ways [18]. We incorporated the finite-mass corrections into our code by modifying the $n \leftrightarrow p$ rates at each temperature by the correction shown in Fig. 9. The resulting correction to Y_P was found to be $\delta Y_P/Y_P = 0.50\%$, valid for $10^{-10} \leq \eta \leq 10^{-9}$.

3.3 Finite-Temperature Radiative Correction

Finite-temperature modifications to the weak rates arise from several sources:

1. the $(1 \pm f)$ quantum statistical factors in the integration over phase space
2. a shift in the electron mass
3. a change in the neutrino-to-photon temperature ratio

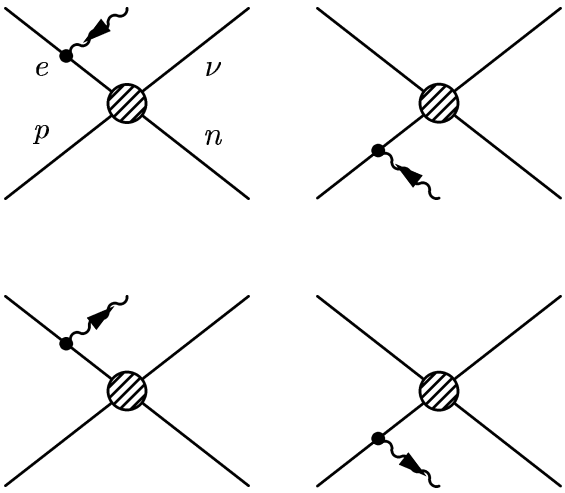

Figure 10: Finite-temperature corrections to the weak rates, i.e., corrections involving photons from the plasma. The bottom two diagrams represent stimulated emission.

4. a correction to the photon and fermion propagators

5. the square of the sum of diagrams for processes that involve photons from the plasma (absorption and stimulated emission); see Fig. 10.

6. finite-temperature wave-function renormalization

Item 1 is included in our definition of the Coulomb correction. We shall define items 2 and 3 to be part of the thermodynamics effects, considered later. Therefore, the finite-temperature radiative correction to the weak rates involves items 4, 5 and 6.

Dicus, et al [8], and Cambier, Primack and Sher [38] calculated the finite-temperature radiative corrections to the weak rates. Neither of these papers correctly handle the finite-temperature wave-function renormalization. In fact, finite-temperature wave-function renormalization is still an open issue. The difficulty lies in the fact that finite temperature spoils Lorentz covariance through the existance of a preferred, thermal frame (in this frame the phase-space distributions are the Bose-Einstein or Fermi-Dirac distributions). The usual methods for obtaining the wave-function renormalization rely on Lorentz covariance, so that the appropriate generalization to the finite-temperature case is not clear. Donoghue and Holstein [9, 10] start by assuming a finite-temperature spinor field – with creation and annihilation operators obeying the standard anti-commutation relations – that satisfies the nonlinear Dirac equation. They write the propagator in terms of these finite-temperature scalars, obtaining a finite-temperature wave-function renormalization that is a multiplicative factor. Sawyer [12], and Esposito, et. al. [39], start by identifying particle states with poles of the propagator, without reference to the finite-temperature field. They assume that the poles are only perturbatively shifted from their zero-temperature values. They then identify the finite-temperature wave-function remormalization with the residue of the propagator at the new pole. The result is a finite-temperature wave-function renormalization that contains additional, non multiplicative terms, so that the results of the two alternative approaches are

process	lower u-limit	upper u-limit	ϵ-Fermi 1	ϵ-Fermi 2	ν	$N(\pm\nu)$
$\epsilon n \to \nu p$	x	∞	$N(u)$	$N(v)$	$w+q$	$-\nu$
$\epsilon p \to \nu n$	q	∞	$N(u)$	$N(v)$	$w-q$	$-\nu$
$\nu n \to \epsilon p$	q	∞	$N(-u)$	$N(-v)$	$w-q$	$+\nu$
$\nu p \to \epsilon n$	x	∞	$N(-u)$	$N(-v)$	$w+q$	$+\nu$
$n \to p\epsilon\nu$	x	q	$N(-u)$	$N(-v)$	$-w+q$	$-\nu$
$p\epsilon\nu \to n$	x	q	$N(u)$	$N(v)$	$-w+q$	$+\nu$

Table 5: Substitutions in Eqs. (21–25) for computing finite-temperature radiative corrections.

different (as pointed out by Chapman [13]). Furthermore, the results of the Sawyer differ from Esposito, et. al., even though they follow similar approaches. The differences change the rates for some processes. *However, for the case of the weak rates, the three different finite-temperature wave-function renormalization results give the same contribution to the weak rates.* For convenience, we used the formalism of Sawyer in our treatment. The resulting correction to the $\epsilon n \to \nu p$ is given as

$$\begin{aligned}\delta\Gamma &= \frac{\epsilon^2 T^4}{2^4\pi^5} G_F^2 \left(1+3g_A^2\right) \times \\ &\int_0^\infty \int_x^\infty du\, dk_v\, p_u N_+(u) \left[N_-(k_v) W_\gamma(u,k_v) + N_+(v) W_r(u,k_v)\right], \end{aligned} \tag{21}$$

where $x = m/T$, $p_u = \sqrt{u^2 - x^2}$, $v = \sqrt{k_v^2 + x^2}$, $N_\pm(u) = 1/(e^u \pm 1)$,

$$\begin{aligned} W_\gamma(u,k_v) &= \left[\left(\frac{k_v}{2p_u} + \frac{u^2}{k_v p_u} \ln\frac{u+p_u}{u-p_u} - \frac{2u}{k_v}\right)\right] \left[H(u+k_v) + H(u-k_v) - 2H(u)\right] + \\ &\left[\frac{u}{p_u}\ln\frac{u+p_u}{u-p_u} - 2\right] \left[H(u+k_v) - H(u-k_v)\right] \end{aligned} \tag{22}$$

$$W_r(u,k_v) = \frac{k_v H(u)}{4p_u v}\left[2u \ln\frac{p_u+k_v}{p_u-k_v} + v\ln\frac{m^4 - (uv - p_u k_v)}{m^4 - (uv + p_u k_v)} - \frac{4k_v p_u u}{p_u^2 - k_v^2}\right] \tag{23}$$

and

$$H(w) = \nu^2 N(-\nu)\Theta(\nu), \tag{24}$$

$$\nu = (w+q) \tag{25}$$

with $q = Q/T$. The term proportional to W_r is due to finite-temperature wave function renormalization. To find the correction to the other weak rates, make the substitutions shown in Table 5.

We calculated the finite-temperature radiative corrections to each of the weak rates. The correction to the summed $n \leftrightarrow p$ rates, which match Sawyer's results, are shown in Fig. 11. The correction formulas are complicated enough to preclude direct incorporation into our BBN code. Therefore we implemented these corrections as temperature-dependent fits within the BBN code. The resulting change in Y_P, $\delta Y_P/Y_P = 0.12\%$, was found to be insensitive to η in the range $10^{-10} \le \eta \le 10^{-9}$. Sawyer claims a change of $+0.02\%$, while Chapman claims a change of $+0.01\%$. Both Sawyer and Chapman compute the change in the neutron fraction to estimate $\delta Y_P/Y_P$. To

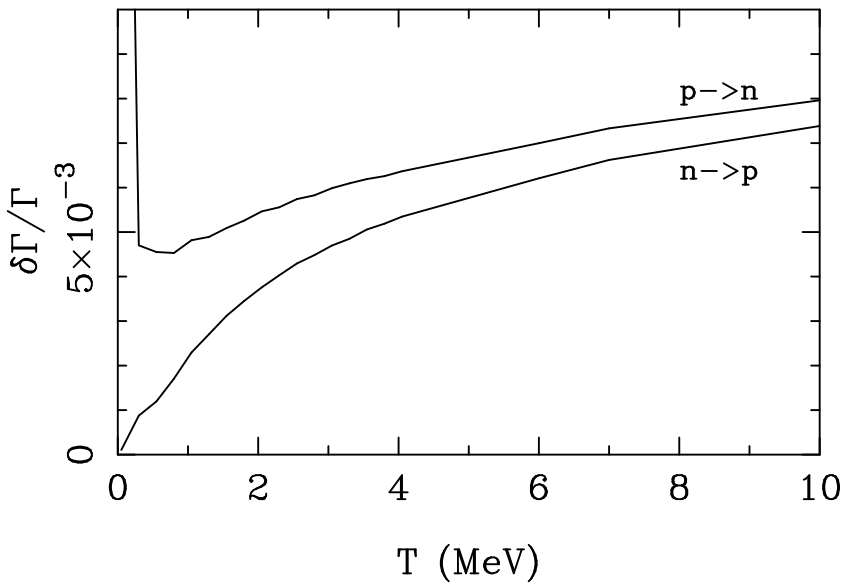

Figure 11: Finite-temperature radiative corrections to the $n \leftrightarrow p$ rates. This plot is to be compared to Fig. 4 in Ref. 12.

first order in the perturbation, the equations governing the evolution of the neutron fraction X_n and its perturbation δX_n, can be written

$$\begin{aligned} \frac{dX_n}{dT} &= \frac{dt}{dT}\left[-X_n\Gamma_{n\to p} + (1-X_n)\,\Gamma_{p\to n}\right] \\ \frac{d\,\delta X_n}{dT} &= \frac{dt}{dT}\left\{\Gamma_{n\to p}\left(\delta X_n + \gamma_n X_n\right) + \Gamma_{p\to n}\left[\gamma_p\left(1-X_n\right) - \delta X_n\right]\right\}, \end{aligned} \tag{26}$$

where $\gamma_n = \delta\Gamma_{n\to p}/\Gamma_{n\to p}$ and $\gamma_p = \delta\Gamma_{p\to n}/\Gamma_{p\to n}$. Then the change in Y_P is estimated as

$$\frac{\delta Y_P}{Y_P} \simeq \left.\frac{\delta X_n}{X_n}\right|_{onset\ of\ BBN} \simeq \left.\frac{\delta X_n}{X_n}\right|_{T=0}. \tag{27}$$

In order to have a direct comparison with the results of Sawyer and Chapman, we found $\delta Y_P/Y_P$ using this method. The evolution of δX_n is shown in Fig. 12. Our results obtained from this approximation method confirm those where we used the BBN code, and differ from Sawyer and Chapman. However, all agree the change in Y_P is small.

4 Thermodynamics

Thermodynamic corrections refer to corrections to the density, pressure and neutrino-to-photon temperature ratio. There are two effects to consider: finite-temperature QED corrections to the equation of state of the electromagnetic plasma, and incomplete neutrino decoupling.

4.1 Finite-temperature QED Correction

The finite-temperature QED corrections encompass corrections to the density, neutrino temperature and electron mass. All of the these corrections follow from the finite-temperature QED modification

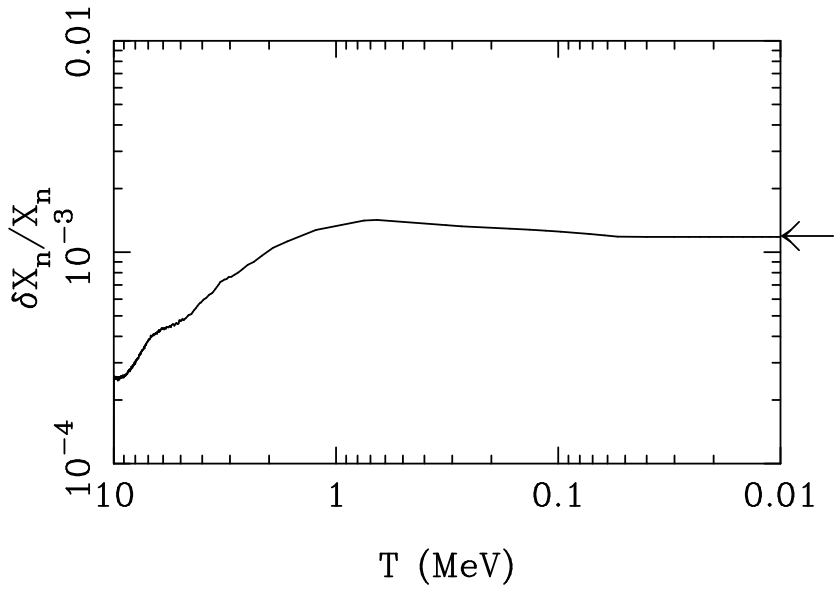

Figure 12: Temperature evolution of the estimated change in neutron fraction X_n due to finite-temperature radiative corrections. The solid line shows the results of integrating the perturbation equations; the low-temperature asymptotic solution gives the correction to Y_P, $\delta Y_P/Y_P = \delta x_n/x_n$. The arrow indicates the final result of substituting the radiative corrections into our full code, expressed as $\delta x_n/x_n$. The two methods agree very well.

to the equation of state of the electromagnetic plasma. These corrections were calculated by Heckler [16] and applied to cosmology and solar physics. We will follow his approach, correcting a few small errors.

Helium is sensitive to thermodynamic quantities in several ways. First, the energy density determines the expansion rate; changes in the expansion rate affect the freeze-out temperature, the abundance of free neutrons, and finally Y_P. The next two effects follow from corrections to the electron mass. First, a change in the electron mass affects the weak rates directly. Second, it changes the entropy of the electron-positron plasma at the time neutrinos decouple; since this entropy is transferred to the photons when the $e^{\pm}$ pairs disappear, this changes the neutrino-to-photon temperature ratio, which affects the weak rates, since they are very sensitive to the neutrino temperature.

The finite-temperature QED correction to the equation of state can be expressed as a modification to the pressure of the pressure-weighted, effective number of effective degrees of freedom,

$$P(T) = P_0(T) + \delta P(T), \tag{28}$$

where $\delta P(T)$ is the correction to the pressure and $P_0(T) = (\pi^2/90)\, g_P T^4$ is the standard expression for the pressure in terms of g_P. The change in pressure can be equated to a change in g_ρ, $\delta g_P = 90/(\pi^2 T^4)\, \delta P$. The correction $\delta P(T)$ can be expressed as an expansion in electron charge $\epsilon \simeq 0.301$: $\delta P(T) = \sum_i \delta P_i(T)$. The Feynman diagrams for the ϵ^2-term and ϵ^3-term are shown in Fig. 4.1.

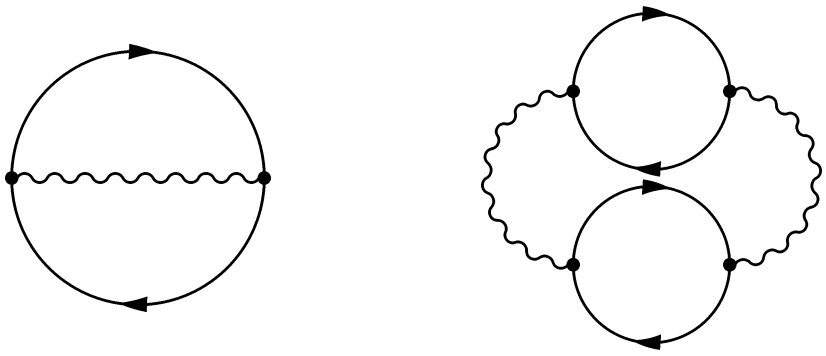

Figure 13: Feynman diagrams that contribute to the correction to the equation of state of the electromagnetic plasma. The left diagram produces the order e^2 correction, while the right diagram is the smaller e^3 correction.

For vanishing chemical potential the e^2 term is [40],

$$\begin{aligned}\delta P_2(T) &= -\frac{e^2T^4}{6\pi^2}\int_x^\infty du\,\frac{\sqrt{u^2-x^2}}{e^u+1} \\ &\quad -\frac{e^2T^4}{8\pi^3}\int_x^\infty\int_x^\infty du\,dv\,p_u\,p_v\,N(u)\,N(v)\left(4+\frac{x^2}{p_u\,p_v}\ln\frac{u\,v+p_u\,p_v+x^2}{u\,v-p_u\,p_v+x^2}\right), \end{aligned} \tag{29}$$

where $x\equiv m_e/T$, $u\equiv E_u/T$, $p_u\equiv\sqrt{u^2-x^2}$ and $N(u)=1/(1+e^u)$. In the high-temperature limit $T\gg m_e$,

$$\delta P_2(T)\simeq -\frac{5e^2T^4}{288} \tag{30}$$

A similar but more involved calculation yields the result for $\delta P_3(T)$ in the limit $T\gg m$ [40],

$$\delta P_3(T)\simeq -\frac{e^3T^4}{36\sqrt{3}\pi}. \tag{31}$$

At high temperatures, the ratio

$$\frac{\delta P_2(T)}{\delta P_3(T)}\simeq\frac{1}{e}\,\frac{\sqrt{3}\pi}{2}\simeq 11, \tag{32}$$

while both the e^2 and the e^3-terms are exponentially suppressed for $T\ll m$. Therefore, to good approximation, we can neglect $\delta P_3(T)$ for all T. For $T\gg m_e$, $\delta g_\rho=-25e^2/16\pi^2$.

From the standard thermodynamic relation $\rho=-P+T\,(\partial P/\partial T)$ we can find the thermodynamic correction to the density, $\rho=\rho_0+\delta\rho$, where the standard density ρ_0 may be written in terms of the density-weighted effective number of relativistic degrees of freedom, $\rho_0=(\pi^2/30)\,g_\rho T^4$. The change in the density can be written

$$\delta g_\rho=\frac{30}{\pi^2T^4}\left(-\delta P+T\,\frac{\partial}{\partial T}\delta P\right)\overrightarrow{T\gg m_e}-\frac{25}{16\pi^2}e^2\,. \tag{33}$$

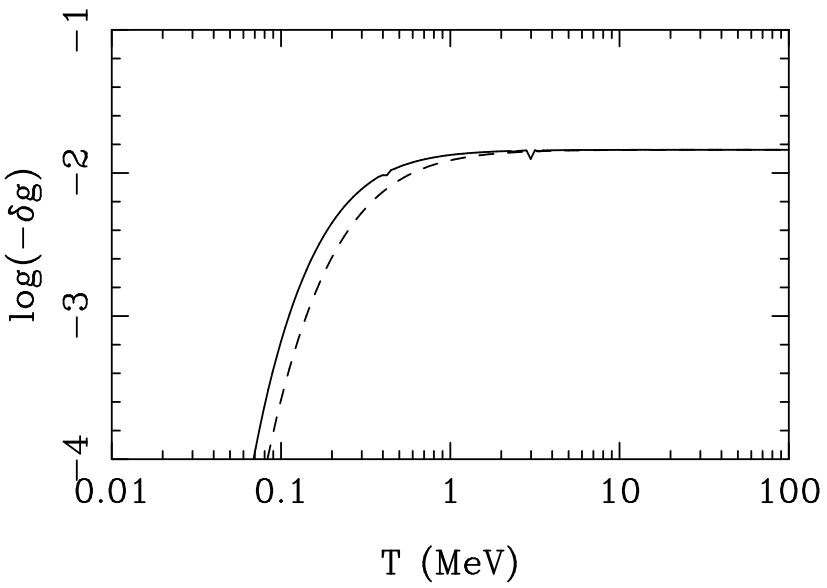

Figure 14: Finite-temperature QED change in pressure-weighted (solid line) and density-weighted (dashed line) relativistic degrees of freedom.

Figure 14 shows δg_ρ and δg_P as a function of temperature.

The finite-temperature QED correction to the pressure is a change in the dispersion relation of the electrons which can be attributed to a change in the electron mass:

$$E^2 = p^2 + m^2 + \delta m^2. \tag{34}$$

The formula for δm^2 follows from the definition of the pressure [40].

$$\begin{aligned} \delta m^2(p,T) &= \frac{\epsilon^2 T^2}{6} + \frac{\epsilon^2 T^2}{\pi^2}\int_x^\infty du\,\frac{k_u}{u}\frac{1}{e^u+1} \\ &\quad -\frac{\epsilon^2 m^2 T}{2\pi^2 p}\int_x^\infty du\,\ln\left|\frac{p_u+k_u}{p_u-k_u}\right|\frac{1}{e^u+1}, \end{aligned} \tag{35}$$

where $x = m_e/T$, $k_u = \sqrt{u^2 - x^2}$ and $p_u = p/T$. Figure 15 shows the finite-temperature QED correction to the electron mass as a function of temperature. Figure 16 shows the effect of the shift in the electron's mass on the $n \leftrightarrow p$ rates. The lower curves indicate the error due to not including the momentum-dependent part of the mass correction. For our calculations, the error is negligable and we neglect the p-dependent term in the mass correction formula.

The final effect of the thermodynamic corrections is a change in the neutrino-to-photon temperature ratio. This can be derived starting with the expression for $\delta P(T)$ and tracking the entropy density of the neutrinos and other particles. Let s_ν be the entropy density of neutrinos and $s_{\rm EM}$

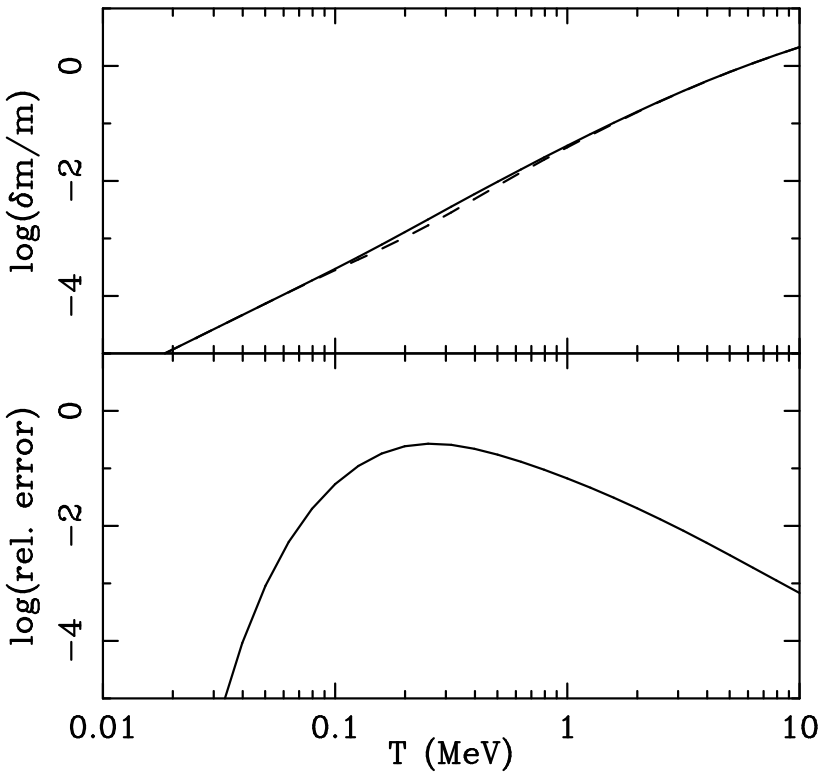

Figure 15: The top panel shows the finite-temperature QED correction to the electron mass as a function of temperature. The dashed curve neglects the p-dependent term, while the solid curve assumes $p = 3\,T$. The bottom panel shows the relative error due to not including the p-dependent term. This error, which is a ten percent correction to the correction, can be safely neglected.

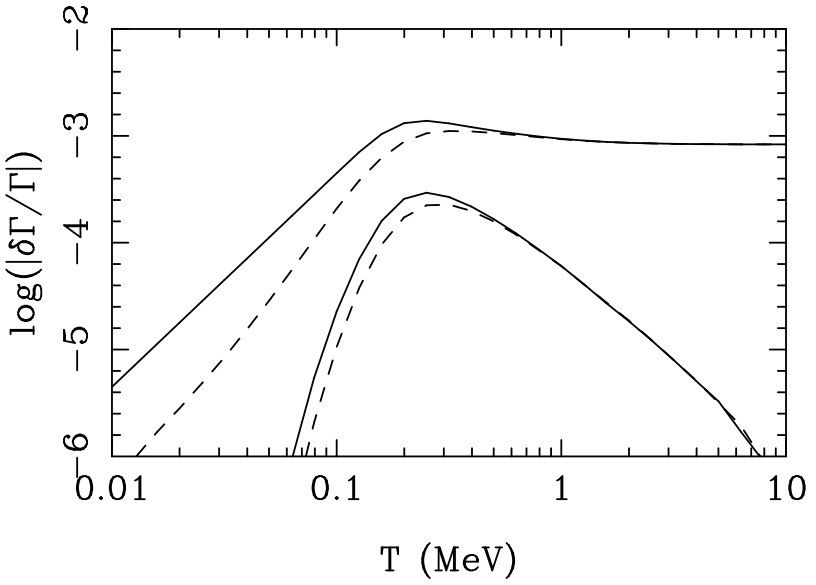

Figure 16: The top curves show the effect of the finite-temperature electron-mass correction on weak rates. The solid curve is for the $n \to p$ rates and the dashed curve is for the $p \to n$ rates. The bottom curves show the error due to not including the p-dependent term in the mass correction formula.

be the combined entropy density of the electrons, positrons and photons:

$$s_\nu = \frac{P_\nu + \rho_\nu}{T_\nu} = \frac{7\pi^2}{30} T_\nu^3, \tag{36}$$

$$s_{\rm EM} = \frac{P_{e^\pm} + \rho_{e^\pm} + P_\gamma + \rho_\gamma}{T}$$

$$= T^3 \left[\frac{4\pi^2}{45} + \frac{2}{3\pi^2} \int_x^\infty du \, \frac{\sqrt{u^2 - x^2}}{e^u + 1} \left(4u^2 - x^2\right) + \frac{\pi^2}{90} \left(\delta g_P + 3\delta g_\rho\right) \right]. \tag{37}$$

In the limitthat the neutrinos are decoupled, the two entropies per comoving volume are separately conserved: $s_\nu a^3$, $s_{\rm EM} a^3 =$ constant, where a is the scale factor. The small residual coupling of the neutrinos to the electromagnetic plasma leads to a correction of about $\sim 0.1\%$ [19], discussed below. At high temperature we have

$$\left. \frac{s_{\rm EM} a^3}{s_\nu a^3} \right|_{T \gg m_e} = \frac{22}{21} + \frac{1}{21} \left[\delta g_P(T) + 3\delta g_\rho(T) \right] \simeq \frac{22}{21} \left(1 - \frac{25}{88} \frac{\epsilon^2}{\pi^2} \right), \tag{38}$$

while for all temperatures,

$$\frac{s_{\rm EM} a^3}{s_\nu a^3} = \left(\frac{T}{T_\nu} \right)^3 \left[\frac{8}{21} + \frac{20}{7\pi^4} \int_x^\infty du \, \frac{\sqrt{u^2 - x^2}}{e^u + 1} \left(4u^2 - x^2\right) + \frac{1}{21} \left[\delta g_P(T) + 3\delta g_\rho(T) \right] \right]. \tag{39}$$

Assuming that the neutrinos decouple at a temperature $T_D \sim 2$ MeV $\gg m_e$ and taking the ratio of entropies to be given by Eqn. (38), it follows that the ratio of the neutrino-to-photon temperature is

$$\left(\frac{T_\nu}{T} \right)^3 = \frac{\frac{4}{11} + \frac{30}{11\pi^4} \int_x^\infty du \frac{\sqrt{u^2 - x^2}}{e^u + 1} \left(4u^2 - x^2\right) + \frac{1}{22} \left[\delta g_P(T) + 3\delta g_\rho(T) \right]}{1 - \frac{25\epsilon^2}{88\pi^2}}, \tag{40}$$

$$\xrightarrow[T \ll m_e]{} \frac{4}{11} \left(1 + \frac{25\epsilon^2}{88\pi^2} \right) \simeq 1.002 \left(\frac{4}{11} \right). \tag{41}$$

The zero-temperature limit of the neutrino temperature photon temperature relation is altered[3]. This makes sense physically: the positive correction to the electron mass means that the electron-positron plasma has less entropy to give to the photons upon annihilation, and thus photons are heated less than they would be without the correction. Figure 17 shows the finite-temperature QED change in neutrino temperature versus photon temperature.

We incorporated the QED corrections to the equation of state into our code by changing the energy densigy, the electron mass in the weak-rate calculations and the neutrino temperature. The resulting change in Y_P, $\delta Y_P / Y_P = +0.043\%$ was found to be insensitive to η in the range, $10^{-10} \leq \eta \leq 10^{-9}$. Dicus, et al [8] attempted to calculate the thermodynamic corrections, and found $\delta Y_P / Y_P = -0.04\%$, but only included the effect of the electron mass on the weak rates. Heckler estimated the effect on Y_P and found $\delta Y_P / Y_P = +0.06\%$. Not only was this just an estimate, but also his value for the change in neutrino temperature is not correct. In any event, the thermodynamic correction to Y_P is small.

[3]This expression differs somewhat from the result obtained by Heckler [16].

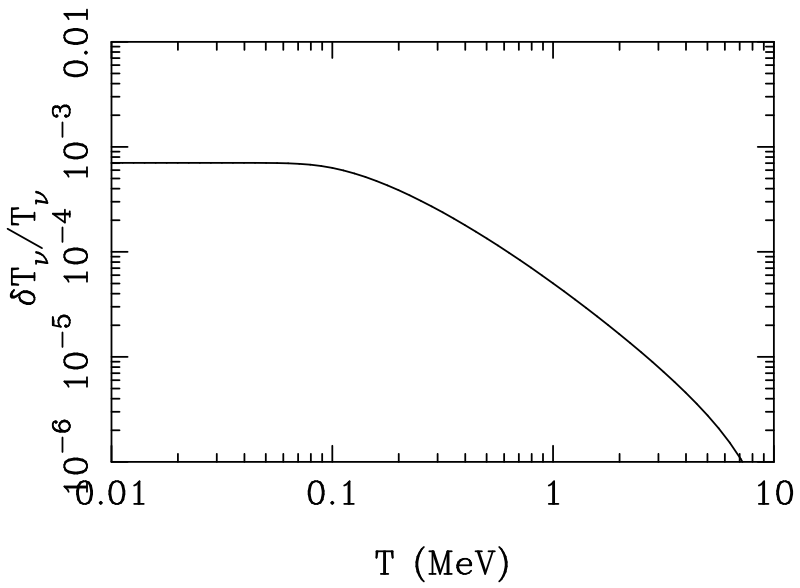

Figure 17: Relative finite-temperature QED change in the neutrino temperature, as a function of photon temperature. Note that the zero-temperature limit is altered from the standard value.

4.2 Incomplete Neutrino Decoupling

The standard code assumes that neutrinos decoupled completely before $e^{\pm}$ annihilations. It has been pointed out that this assumption is not strictly valid [8]. Neutrinos are "slightly coupled" when $e^{\pm}$ pairs are annnihilated, and hence share somewhat in the heat released. The first calculations [8, 41, 42] of this effect were "one-zone" estimates that evolved integrated quantities through the process of neutrino decoupling. More refined "multi-zone" calculations tracked many energy bins, assumed Boltzmann statistics and made other approximations. [19, 43]. The latest refinements have included these small effects as well [44, 45, 46]. Fields et al [47] incorporated the slight effect of the heating of neutrinos by $e^{\pm}$ annililations into the standard code and found a shift in ^{4}He production, $\delta Y_P = +1.5 \times 10^{-4}$, which is insensitive to η for $10^{-10} \leq \eta \leq 10^{-9}$.

5 Summary

All of the physics corrections we investigated have been studied elsewhere. However, not all of them have been implemented in a full code; there have been changes in some of the physics corrections, and the issue of numerical accuracy has not been studied thoroughly. Further, the corrections have been implemented in a patchwork fashion, so that the users of many codes do not know which corrections are in, which are out, and which may be double counted (e.g., adding the Kernan-Krauss numerical correction and running a small stepsize).

The goal of this work was a calculation of the primordial ^{4}He abundance to a precision limited primarily by the uncertainty in the neutron mean lifetime, $\delta\tau_n = \pm 2$sec, or $\delta Y_P/Y_P \simeq 0.1\%$, with reliable estimates of the theoretical error. To achieve this goal we created a new BBN code, designed, engineered and tested to this numerical accuracy. To this baseline code we added the

	Y_P	Cumulative δY_P ($\times 10^{-4}$)	Cumulative $\delta Y_P/Y_P$ (%)	Effect Alone δY_P ($\times 10^{-4}$)	Effect Alone $\delta Y_P/Y_P$ (%)
Baseline	0.2411				
Coulomb and $T=0$ radiative	0.2442	+31	+1.28	+31	+1.28
finite mass	0.2454	+43	+1.78	+12	+0.50
finite T radiative	0.2457	+46	+1.90	+3	+0.12
QED plasma	0.2458	+47	+1.94	+1	+0.04
residual ν-heating	0.2460	+49	+2.00	+1.5	+0.06

Table 6: Summary of results. For absolute numbers we have picked $\eta = 5.0 \times 10^{-10}$. By baseline we mean the results of our BBN code without any of the physics effects listed, and with small numerical errors.

microphysics necessary to achieve our accuracy goal – Coulomb and zero-temperature radiative corrections, finite-nucleon-mass corrections, finite-temperature radiative corrections, QED thermodynamical corrections, and the slight heating of neutrinos by $e^{\pm}$ annihilations. These corrections – coincidentally all positive – increase the predicted ^{4}He abundance by $\delta Y_P = 0.0048$ or 2%. Table 6 summarizes these corrections for $\eta = 5 \times 10^{-10}$. (We chose this value for η because it is the central value implied by recent measurements of the deuterium abundance in high-redshift hydrogen clouds [35, 48, 49].) Summarizing our work in one number

$$Y_P(\eta = 5 \times 10^{-10}) = 0.2459 \pm 0.0004 \text{ (expt)} \ \pm < 0.0002 \text{ (theory)}. \tag{42}$$

Finally, we give two fitting formulae for our high-accuracy ^{4}He predictions. The first, is accurate to better than 0.1% and is valid for $10^{-10} \leq \eta \leq 10^{-9}$, $N_\nu = 3.00$ and $880\,\mathrm{sec} \leq \tau_n \leq 890\,\mathrm{sec}$. In terms of $\zeta \equiv 10 + \log \eta$,

$$\begin{aligned} Y_P(\zeta, \tau_n) &= Y_P(\zeta, 885.3\,\mathrm{sec}) + (\tau_\mathrm{n} - 885.3\,\mathrm{sec})\,\delta \mathrm{Y_P}(\zeta), \\ Y_P(\zeta, 885.3\,\mathrm{sec}) &= \left(a_0 + a_1\,\zeta + a_2\,\zeta^2 + a_3\,\zeta^3 + a_4\,\zeta^4\right), \\ \delta Y_P(\zeta) &= \left(b_0 + b_1\,\zeta + b_2\,\zeta^2 + b_3\,\zeta^3 + b_4\,\zeta^4\right) \end{aligned} \tag{43}$$

where the coefficients a_i, b_i are given by

$$\begin{aligned} a_0 = 0.22285\,, &\quad a_1 = 0.05418\,, &\quad a_2 = -0.04816\,, \\ &\quad a_3 = 0.02990\,, &\quad a_4 = -0.00578 \\ b_0 = 2.101 \times 10^{-4}\,, &\quad b_1 = -0.406 \times 10^{-4}\,, &\quad b_2 = 2.701 \times 10^{-4}\,, \\ &\quad b_3 = -5.539 \times 10^{-4}\,, &\quad b_4 = 3.295 \times 10^{-4}\,. \end{aligned} \tag{44}$$

The second fitting formula is accurate to 0.5% and is valid for $10^{-10} \leq \eta \leq 10^{-9}$, $880\,\mathrm{sec} \leq \tau_n \leq 890\,\mathrm{sec}$, and $2.5 \leq N_\nu \leq 4.0$.

$$Y_P(\zeta, \tau, N) = Y_P(\zeta, \tau, 3) + (N-3)\left(c_0 + c_1\,\zeta + c_2\,\zeta^2 + c_3\,\zeta^3 + c_4\,\zeta^4\right), \tag{45}$$

where

$$\begin{aligned} c_0 = 0.0111\,, &\quad c_1 = 0.00481\,, &\quad c_2 = -0.01182\,, \\ &\quad c_3 = 0.01474\,, &\quad c_4 = -0.00553\,. \end{aligned} \tag{46}$$

Acknowledgements

The BBN code we described in this paper began as a project for a graduate course in cosmology. R.L. gratefully acknowledges the Red Team, Moses Hohman, Mike Joffre, Russel Strickland and Craig Wiegert. This work was supported in part by the DOE (at Chicago and Fermilab) and by NASA at Fermilab through grant NAG 5–2788.

References

[1] D.N. Schramm and M.S. Turner, Rev. Mod. Phys. **70**, 303 (1998).

[2] J. Yang, M.S. Turner, G. Steigman, D.N. Schramm, and K.A. Olive, Astrophys. J. **281**, 493 (1984).

[3] T.P. Walker et al., Astrophys. J. **376**, 51 (1991).

[4] S. Sarkar, Rep. Prog. Phys. **59**, 1493 (1996).

[5] C.J. Copi, M.S. Turner, and D.N. Schramm, Phys. Rev. D **55** (1997).

[6] V.F. Schvartsman, JETP Lett. **9**, 154 (1969).

[7] G. Steigman, D.N. Schramm, and J. Gunn, Phys. Lett. B **66**, 202 (1977).

[8] D. Dicus et al., Phys. Rev. D **26**, 2694 (1982).

[9] J.F. Donoghue and B.R. Holstein, Phys. Rev. D **28**, 340 (1983).

[10] J.F. Donoghue and B.R. Holstein, Phys. Rev. D **29**, 3004 (1984).

[11] P. Kernan, PhD thesis, Ohio State University, 1993.

[12] R.F. Sawyer, Phys. Rev. D **53**, 4232 (1996).

[13] I.A. Chapman, Phys. Rev. D **55**, 6287 (1997).

[14] M.S. Smith, L.H. Kawano, and R.A. Malaney, Astrophys. J. Suppl. **85**, 219 (1993).

[15] G. Fiorentini, E. Lisi, S. Sarkar, and F. L. Villante, astro-ph/9801377 .

[16] A.J. Heckler, Phys. Rev. D **49**, 611 (1994).

[17] D. Seckel, hep-ph/9305311 (1993).

[18] R.E. Lopez, M.S. Turner, and G. Gyuk, Phys. Rev. D **56** (1997).

[19] S. Dodelson and M.S. Turner, Phys. Rev. D **46**, 3372 (1992).

[20] C. Caso et al., Euro. Phys. J. **C3**, 1 (1998).

[21] P. Geltenbort et al., in *presented at Wein98*, Santa Fe, NM, 1988.

[22] J. Byrne et al., Europhys. Lett. **33**, 187 (1996).

[23] L. Kawano, Fermilab-pub-92/04-a, 1992.

[24] N. Itoh, A. Nishikawa, S. Nozawa, and Y. Kohyama, Astrophys. J. **488**, 507 (1997).

[25] R.V. Wagoner, W. Fowler, and F. Hoyle, Astrophys. J. **148**, 3 (1966).

[26] R.V. Wagoner, Astrophys. J. **179**, 343 (1973).

[27] W.H. Press, S.A. Teukolsky, W.T. Vetterling, and B.P. Flannery, *Numerical Recipes in C*, Cambridge University Press, Cambridge, 1990.

[28] R.V. Wagoner and D.N. Schramm, Ann. Rev. Nucl. Part. Sci. **27**, 37 (1977).

[29] L. Kawano, Fermilab-pub-88/34-a, 1988.

[30] P.J. Kernan and L.M. Krauss, Phys. Rev. Lett. **72**, 3309 (1994).

[31] L. Krauss and P. Romanelli, Astrophys. J. **358**, 47 (1990).

[32] L.M. Krauss and P.J. Kernan, Astrophys. J. Lett. **432**, 79 (1994).

[33] N. Hata et al., Phys. Rev. Lett. **75**, 3977 (1995).

[34] S. Burles, K. Nollett, J. Truran, and M.S. Turner, in preparation (1998).

[35] S. Burles and D. Tytler, Astrophys. J. **499**, 699 (1998).

[36] S. Weinberg, *Gravitation and Cosmology*, J. Wiley, New York, 1972.

[37] D.H. Wilkinson, Nucl. Phys. A **377**, 474 (1982).

[38] J. Cambier, J.R. Primack, and M. Sher, Nucl. Phys. B **209**, 372 (1982).

[39] S. Esposito, G. Mangano, G. Miele, and O. Pisanti.

[40] J.I. Kapusta, *Finite-Temperature Quantum Field Theory*, Cambridge University Press, Cambridge, 1989.

[41] M. A. Herrera and S. Hacyan, Astrophys. J. **336**, 539 (1989).

[42] N. C. Rana and B. Mitra, Phys. Rev. D **44**, 393 (1991).

[43] A. D. Dolgov and M. Fukugita, Phys. Rev. D **46**, 5378 (1992).

[44] N.Y. Gnedin and O.Y. Gnedin, astro-ph/9712199 .

[45] S. Hannestad and J. Madsen, Phys. Rev. D **52**, 1764 (1995).

[46] A. D. Dolgov, S. H. Hansen, and D.V. Semikoz, Nucl. Phys. B **503**, 426 (1997).

[47] B. Fields, S. Dodelson, and M.S. Turner, Phys. Rev. D **47**, 4309 (1993).

[48] S. Burles and D. Tytler, Astrophys. J. , in press (1998).

[49] S. Burles and D. Tytler, astro-ph/9712265 (1997).